

ISSN: 2770-6613



\*Corresponding authors: Xiangyang Hao, Jingang Liu and Yihe Zhang, Engineering Research Center of Ministry of Education for Geological Carbon Storage and Low Carbon Utilization of Resources, Beijing Key Laboratory of Materials Utilization of Nonmetallic Minerals and Solid Wastes, National Laboratory of Mineral Materials, Hebei Key Laboratory of Resource Low-carbon Utilization and New Materials, School of Materials Science and Technology, China University of Geosciences (Beijing), China

**Submission:** 

☐ October 23, 2025 **Published:** 
☐ November 07, 2025

Volume 6 - Issue 2

How to cite this article: Xiangyang Hao\*, Liang Wu, Chao Zhang, Da Chen, Yonglong Zhang, Mingzhang Sun, Jijin Mu, Jingang Liu\* and Yihe Zhang\*. Ternary Composite for Deep-Sea Oil Pipelines Thermal Insulation Belt. Polymer Sci peer Rev J. 6(2). PSPRJ. 000632. 2025.

DOI: 10.31031/PSPRJ.2025.06.000632

Copyright@ Xiangyang Hao, Jingang Liu and Yihe Zhang, This article is distributed under the terms of the Creative Commons Attribution 4.0 International License, which permits unrestricted use and redistribution provided that the original author and source are credited.

# **Ternary Composite for Deep-Sea Oil Pipelines Thermal Insulation Belt**

Xiangyang Hao<sup>1\*</sup>, Liang Wu<sup>2</sup>, Chao Zhang<sup>1</sup>, Da Chen<sup>1</sup>, Yonglong Zhang<sup>1</sup>, Mingzhang Sun<sup>1</sup>, Jijin Mu<sup>1</sup>, Jingang Liu<sup>1\*</sup> and Yihe Zhang<sup>1\*</sup>

<sup>1</sup>Engineering Research Center of Ministry of Education for Geological Carbon Storage and Low Carbon Utilization of Resources, Beijing Key Laboratory of Materials Utilization of Nonmetallic Minerals and Solid Wastes, National Laboratory of Mineral Materials, Hebei Key Laboratory of Resource Low-carbon Utilization and New Materials, School of Materials Science and Technology, China University of Geosciences (Beijing), China

<sup>2</sup>School of Electronics, Peking University, China

#### **Abstract**

In recent years, the exploration of offshore oil and gas resources in deep waters has notably increased. This has increased the demand for undersea thermal insulation belt for Deep-sea Oil Pipelines with high performance. Polypropylene (PP) is an environmentally friendly and recyclable material. However, its mechanical properties and thermal insulation performance inherently limit its application in deep waters. Herein, a ternary composite was prepared by modifying Hollow Glass Bead (HGB) with KH-550 and PP-coated glass fiber (CGF). The prepared composite exhibits excellent mechanical properties and favorable thermal insulation characteristics. Industrial-grade product belt has been produced by using a two-step process with optimizing machining parameters. The material prepared with 20% HGB and 1% GF exhibited compressive strength, compressive modulus, and thermal conductivity of 91.24MPa, 629.05MPa, 0.1W/m·K, respectively. These values exceed the standards for deep-sea oil pipelines belt.

**Keywords:** Hollow Glass Bead (HGB); Polypropylene (PP); Glass Fiber (GF); Thermal Insulation Properties

# Introduction

With increasing global energy demand and gradual depletion of terrestrial oil and gas resources, the development of deep-sea oil and gas resources is crucial [1]. Additionally, with advances in deep-sea oilfield development and extraction technologies, undersea oil pipelines are the predominant method for offshore oil and gas transportation. However, the harsh conditions in deep-sea environments present severe challenges to the thermal insulation of undersea pipelines. Factors such as variations in seawater temperature, high pressure, and complex seabed terrain complicate drilling and extraction, increasing the requirements for oil and gas transportation pipelines, particularly regarding thermal insulation systems [2,3]. When oil and natural gas are extracted and transferred from the bottom to land, the temperature of the transport medium steadily decreases. Substances with higher solidification points, such as paraffin, precipitate first, whereas the viscosity of substances such as asphaltene rapidly increase [4,5], leading to pipeline blockages, safety incidents, and economic losses [6]. Therefore, thermal insulation systems should be added to oil pipelines to maintain the temperature of the transported medium. In addition, the hydrostatic pressure is high in deep-sea environments. Reportedly, composites containing a polymer matrix with low ultraviolet sensitivity and inorganic particles or fibers as reinforcement can be used as thermal insulation layers for oil pipelines [7].

The most frequently used matrix materials in oil pipeline thermal insulation systems are Polyurethane (PU) [8], Epoxy Resin (EP) [7,9], and PP [10]. PU is a highly insulating and

abrasion-resistant material mostly used in shallow and mediumdepth thermal insulation performance sea pipelines. However, PU materials exhibit limitations in deep-sea environments, primarily because of their susceptibility to compression deformation under high pressure and high cost, which prevents their use in deepsee environments. In contrast, although EP materials offer high mechanical strength and chemical resistance, the relatively high open-cell content in their foam structure results in increased thermal conductivity and water absorption, unfavourable for maintaining oil and gas transport. PP has emerged as a promising material for thermal insulation systems for undersea oil and gas pipelines because of several factors, including environmental compatibility, recyclability, and cost-effectiveness. The Thunderhorse oil field in the Gulf of Mexico [11] uses a seven-layer PP coating system for thermal insulation at a depth of 2,000m. The system employs either HGB reinforced PP resin or PP foam as the insulation layer, along with UV-resistant PP as the protective layer.

An analysis of the thermal insulation systems of submarine oil pipelines reveals that the PP thermal insulation material offers several advantages, including a lightweight composition, low water absorption, easy installation and repair, and minimal cost. Its usage is suitable at water depths >3,000m, and it exhibits excellent thermal resistance and can maintain integrity for products at approximately 120 °C. Notably, three principal categories of thermal insulation materials derived from PP are employed in the construction of undersea oil pipelines. These materials are foamed, solid, and composite PP [12]. Foamed PP has not progressed as quickly as the other two types because of its low melt strength, which makes it susceptible to pore collapse and making it difficult to control the foam quality. Solid PP can be used continuously in deep-sea environments exceeding 3,000m and can withstand temperatures up to 140 °C. However, solid PP exhibits substantially worse thermal insulation effects, which can lead to aging and limit its application in undersea environments.

Composite PP thermal insulation materials are fabricated by adding inorganic particles to PP. Material modification serves as a pivotal strategy to endow materials with significantly enhanced properties and substantially broaden their application scope [13,14]. An exemplary granule is HGB, which has a hard shell, high strength, corrosion resistance, good thermal insulation, and excellent flowability [15,16]. The gas inside the HGB shells results in low thermal conductivity, which further improves the thermal insulation performance of the composite but diminishes its mechanical qualities [17-19]. HGB/PP composites have been used in undersea oil pipelines; however, their mechanical properties limit their use in deep offshore oil and gas resources. The mechanical strength of HGB/PP materials is relatively low; thus, withstanding the extreme pressures of deep seas for long periods is difficult for these materials. This limitation is particularly evident in deepwater applications, which are prone to deformation or failure, leading to compromising the service life of a pipeline.

This study aims to develop an advanced PP composite incorporating HGB and GF to enhance thermal insulation and mechanical properties for deep-sea applications. It systematically investigates the effects of HGB and GF content variations on composite performance, ultimately providing a high-performance and cost-effective thermal insulation solution specifically designed for deep-sea oil and gas pipelines.

#### **Materials and Methods**

## **Materials**

PP (grade K8303) from Sinopec (China), GF and modified GF (PP-coated GF, abbreviation CGF) from Taishan Fiberglass Inc. (China), HGB (grade iM16K) from 3M (USA) were used in this study. Their key characteristics are summarized in Table 1-3, respectively. The silane coupling agent KH-550 (Guangzhou Zhongjie Chemical Technology Co., Ltd., China) was used as a surface modifier for the HGB, while polypropylene-grafted-maleic anhydride (PP-g-MAH, Shenyang Ketong Plastics Co., Ltd., China) served as a compatibilizer.

Table 1: Parameters of K8303 PP.

Parameters	Melt Flow Rate (g/10min)	Tensile Yield Stress (MPa)	Flexural Modulus (MPa)	Charpy Notched Impact Strength (kJ/m²)
K8303	2.4	23.3	952	49

Table 2: Parameters of GF.

Parameters Line Density (Tex)		Line Density (Vield) Fiber Diameter(µm)		Inhibitor Type	
TCR738	2000	248	13	PP	

Table 3: Parameters of iM16K HGB.

Parameters	Density/g·cm <sup>-3</sup>	Compressive Strength (90%residual)/PSI	Shell Thickness (μm)	Size Distribution (μm)		
				10 <sup>th</sup> %	50 <sup>th</sup> %	90 <sup>th</sup> %
iM16K	0.46	16000	1.34	10	20	30

## **Equipment**

Experimental exploration was carried on twin-screw extruder (model TSE-30A, diameter of 30mm, length-to-diameter (L/D) ratio of 40, Nanjing Ruia Extrusion Machinery Manufacturing

Co., Ltd., China). Industrialized products heat reserving belt were manufactured on high-speed, high-torque, co-rotating parallel twinscrew extruder (model THJ-65, diameter of 65mm, L/D ratio of 52, Nanjing Chengmeng Machinery Co., Ltd., China) and calendering device (model XMHD, Tengzhou Xiangmeng Metal Products Factory,

China). Morphology of the samples were investigated by scanning electron microscope (SEM, model JSM-IT300, JEOL Corporation, Japan). Mechanics performance testing was evaluated on universal testing machine (model CMT4304, MTS Industrial Systems Co., Ltd., China). Thermal conductivity measurement was studied on Thermo Thermal conductivity meter (model TC3100, Xi'an Xiaxi Electronic Technology Co., Ltd., China). Thermal decomposition temperature test was done on Thermogravimetric analysis system (TGA, model STA8000, PerkinElmer Company, USA). Surface smoothness was inspected on Optical microscope (model BX60, Nanjing Yiroda Instrument and Equipment Co., Ltd., China).

#### **Modification of HGB**

A mixed solution was prepared by combining Deionized Water (DI) and Ethanol (EtOH) in a 1:9 volume ratio. Subsequently, the pH of the resulting solution was adjusted to 4 by dropwise adding Hydrochloric Acid (HCI), creating a weakly acidic environment. KH-550 was then added to the prepared solution to form a KH-550-ethanol-water mixture with a specific concentration. The pre-dried HGB were treated with the KH-550-ethanol aqueous solution, with

the amount of KH-550 controlled at 1 wt% relative to the HGB. The mixture was stirred vigorously for 30 minutes. The treated HGB was then transferred to an oven and dried at 105  $^{\circ}$ C for 4 hours before use.

## Sample preparation

**Preparation of HGB/PP composite:** S1 was an unmodified HGB/PP composite, whereas S2 was a modified HGB/PP composite. A total of 20% of dried HGB (both unmodified and modified) was weighed and uniformly mixed with 73.2% PP. The mixture was then fed into a twin-screw extruder. The screw speed and the feed motor frequency of the extruder were set at 17.7Hz and 7.99Hz, respectively, with the latter corresponding to the actual gravimetric feed rate. The temperature profile of the extruder, starting from the I to IX zones, was set as follows: 180 °C, 198 °C, 198 °C, 198 °C, 200 °C, 200 °C, 200 °C, 198 °C, 198 °C. The strip was mould pressed at 150 °C and 15MPa for 30 minutes, then allowed to cool naturally to room temperature (25 °C) under pressure. The test samples were withdrawn for the performance test. Figure 1 illustrates the preparation process.

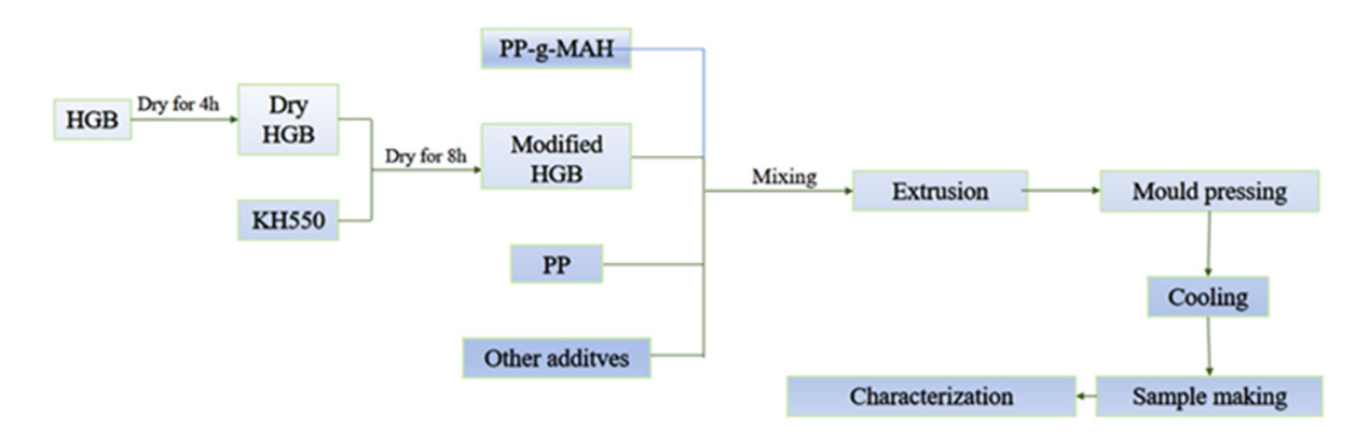


Figure 1: Process flow of hollow glass beads/polypropylene composite.

**Preparation of HGB/GF/PP composite:** Group S3 was HGB/GF/PP composites. PP was mixed with modified HGB and GF (5%, 10%, 15%, 20%, and 25%) using a twin-screw extruder. The extrusion conditions were maintained identical to those described in 2.4.1. The prepared samples were subjected to performance tests.

**Preparation of HGB/PP-coated GF/PP composite:** Group S4 represents the HGB/CGF/PP composite with a modified glass fiber incorporation method. PP-coated GF with different percentages (1%, 3%, 5%, 7%, and 9%) was mixed with PP and modified HGB. The extrusion conditions were kept identical to those described in Section 2.4.1. After extrusion, the properties of the prepared samples were tested.

**Preparation of HGB/PP-coated GF/PP composite using two-step process:** S5 was fabricated using a two-step preparation process. After combining the modified 20% HGB with 1% PP-coated GF and PP were placed inside feeding hopper and main feeding hopper of the extruder respectively, to yield a homogenous strip consisting of HGB, GF, and PP. Subsequently, the extruded mixture was chopped into 5-mm-long masterbatch or slices. The masterbatch was subsequently extruded using a single-screw extruder to fabricate HGB/PP-coated GF/PP composite belt. The extrusion conditions were kept identical to those described in 2.4.1. This process is depicted in Figure 2 & 3.

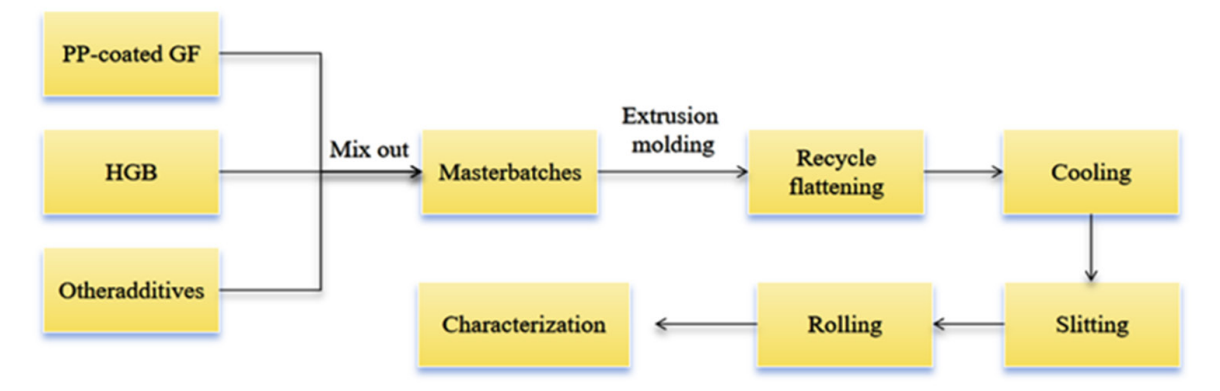


Figure 2: Preparation of HGB/PP-coated GF/PP composite belt.



Figure 3: Industrial production (a) Blending modification extrusion, (b) Masterbatch, (c) Calendering (d) Slit and collection.

## Characterization

SEM observations were performed using a JSM-IT300 microscope (JEOL Ltd., Japan) at an accelerating voltage of 10 kV. For SEM observation, samples with dimensions of approximately 3mm  $\times$  3mm  $\times$  1mm were prepared by cryo-fracturing in liquid nitrogen. The fractured surfaces were sputter-coated with a thin gold layer to enhance conductivity before examination. Optical microscopy was conducted using a BX60 microscope (Nanjing Yiluoda Instrument Equipment Co., Ltd., China) at magnifications ranging from  $100\times$  to  $200\times$ . Undersea applications, more emphasis is placed on compressive resistance performance. Compression tests were carried out on a universal testing machine (CMT4304, MTS Industrial Systems Co., Ltd., China) according to Chinese National

Standard GB/T 1041-2008, which refer to the corresponding ASTM. Compression test specimens were rectangular blocks (10  $\times$  10  $\times$  5mm). All reported mechanical properties represent the average values obtained from five replicate measurements.

Thermal conductivity was determined using a thermal conductivity meter (model TC3100, Xi'an Xiaxi Electronic Technology Co., Ltd., China) in accordance with GB/T 3399-2009, which employs the guarded hot plate method. Two identical specimens were fabricated, each with side lengths ≥80mm and a thickness ranging from 2 to 20mm. Thermogravimetric Analysis (TGA) was performed using a simultaneous thermal analyzer (model STA8000, PerkinElmer, USA). The measurement was carried out under a nitrogen atmosphere at a heating rate of 10 °C/min, within a temperature range of 25 °C to 600 °C.

## Analysis of bubble hole parameters

The integration of HGB into the PP matrix forms air bubble voids inside the composite structure. The distribution and uniformity of these voids substantially affect the overall performance of the composite and can be quantitatively analyzed using specific void parameters. These parameters include void density, diameter, and distribution, elucidating the dispersion effect of the HGB within the PP matrix. To assess these parameters, SEM images of the composite were analyzed using software ImageJ, which facilitates precise statistical analysis by calculating the number and size distribution of bubble holes in the composite [20]. The essential criteria are expressed as follows:

$$N_f = \left(\frac{NM^2}{A}\right)^{3/2} \tag{1}$$

where  $N_{\rm f}$  denotes the hole density /cm³, "N" represents the number of holes in the statistical area, "M" represents the magnification of the EM, and "A" represents the statistical area of the EM photo, cm².

$$\bar{D} = \frac{1}{n} \sum_{1}^{n} D_{I}$$
 (2)

Where  $\bar{D}$  denotes the average particle size ( $\mu$ m), n represents the number of holes, and D<sub>2</sub> denotes various hole diameters( $\mu$ m).

$$S_d = \sqrt{\frac{1}{n} \sum_{i \neq j}^n \left( D_i - \overline{D} \right)^2}$$
 (3)

where  $S_d$  denotes the bubble hole distribution( $\mu m$ ).

## **Result and Discussion**

## Microscopic properties and performance of S1 and S2

As shown in Figures 4(a,b) and Table 4, the interaction between unmodified HGB and PP results in a cell density of  $6.93\times10^6$ 

pores/cm<sup>3</sup> and a porosity of 19.46%, accompanied by inadequate interfacial adhesion. Despite these values, the weak bonding remains a limitation, highlighting the need for improved adhesion mechanisms. The SEM images in Figure 4c, Figure d illustrate that the adhesion of HGB in the PP matrix is considerably enhanced after KH-550 treatment. The HGB were homogeneously dispersed within the matrix. This enhancement is attributed to the addition of KH-550, which improve the interfacial adhesion between PP and HGB. This finding is consistent with reports in the literature [21,22]. The treatment increased the bubble hole density to 1.75×10<sup>8</sup> pores/cm<sup>3</sup> and resulted in a corresponding increase in porosity to 28.09%, as shown in Table 4. These changes indicate improved dispersion and integration. Despite this improved dispersion, some HGB exhibited signs of breakage. This fragility compromises the mechanical properties because the integrity of the HGB is critical for maintaining the desired balance between lightweight characteristics and mechanical properties. Surface modification using KH-550 reduces agglomeration and increases interfacial density, with the mechanical properties being optimal at a 20% HGB mass fraction [23]. As shown in Figure 5, HGB modification enhances the compression properties of the composite. The average compressive modulus of the modified HGB composite (S2, 222.09MPa) was considerably higher than that of the unmodified HGB composite (S1, 158.95MPa). This is because the weak adhesion in S1 causes filler detachment under load, reducing the interface's ability to absorb energy. In contrast, the surface-modified HGB in S2 improves the interfacial bonding with PP, preventing detachment under stress and allowing for more effective energy absorption, thereby improving compression performance. Therefore, further strategies to mitigate HGB breakage could unlock even greater improvements in the mechanical properties of the composite.

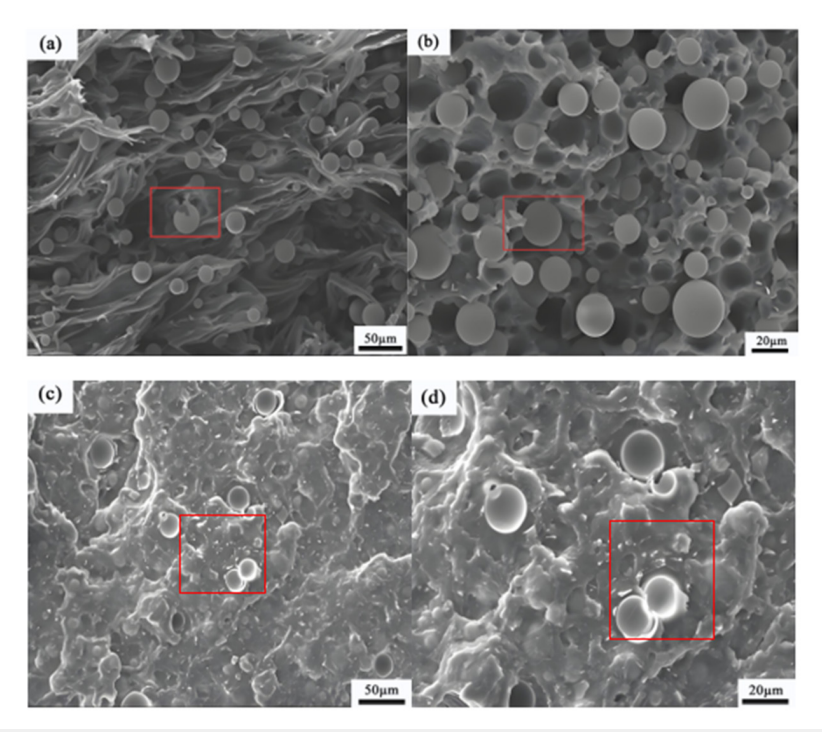


Figure 4: SEM images of unmodified (a, b) and modified (c, d) HGB/PP composites.

Table 4: Pore parameters for S1 and S2.

System	Cell Density (cells/cm <sup>3</sup> )	Average Cell Diameter (µm)	Porosity (%)
S1	6.93×10 <sup>6</sup>	1.36	19.46
S2	1.75×10 <sup>8</sup>	1.30	28.09

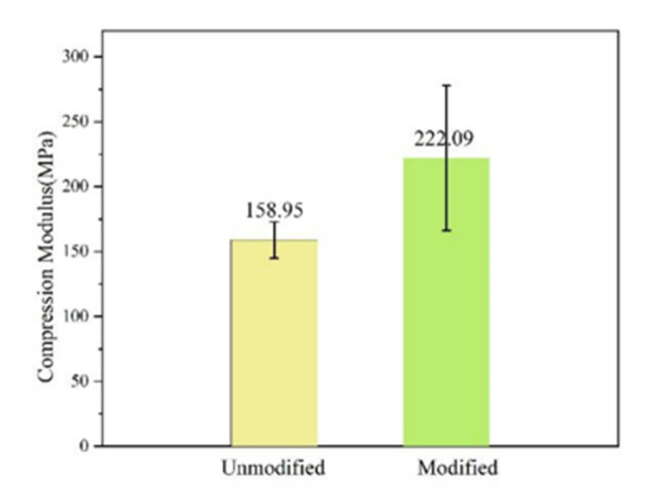


Figure 5: Effect of HGB modification on compression modulus.

## Microscopic properties and performance of group S3

The distribution of HGB and GF in the PP matrix is irregular, and the two components are discernible in the SEM image shown in Figure 6(a). The image depicts a chaotic arrangement of bubble holes, with noticeable cracks and faults in the matrix. Due to the lack of distinguishable and consistent characteristics, bubble pore parameters could not be precisely measured using

ImageJ, complicating quantitative analysis of this heterogeneous microstructure. As the GF content in the composite increased from 5% to 20%, the uniformity of the raw material mixture notably decreased, further complicating the extrusion process. At 25% GF, severe agglomeration of the raw material was observed, making the extrusion difficult. The blockage was caused by agglomerated filler obstructing the inlet, highlighting the processing difficulties associated with excessive filler content.

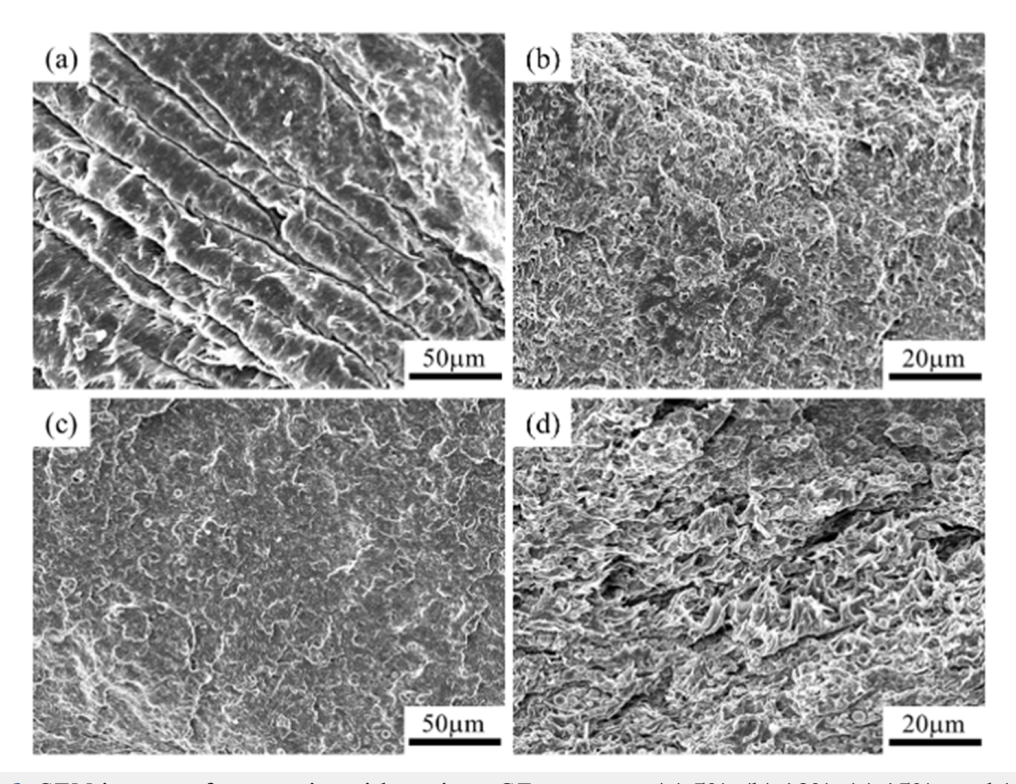
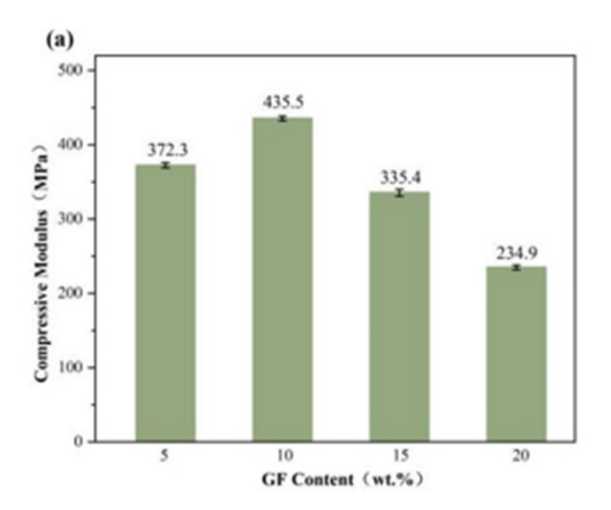
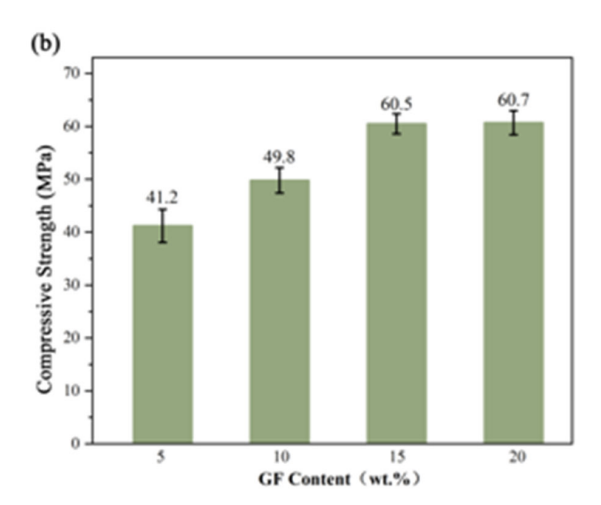


Figure 6: SEM images of composite with various GF contents: (a) 5%, (b) 10%, (c) 15%, and (d) 20%.

Figure 7 shows the compression modulus of Group S3. The compression modulus of Group S3 increases and then decreases for GF contents ranging from 5% to 20%, reaching a maximum value of 435.5MPa at 10% GF. The compression strength of the composite peaked at 60.7MPa at a 20% GF concentration and gradually increased with further GF content. When GF content exceeds 10%, the fillers begin to agglomerate, leading to nonuniform dispersion of GF in PP, which prevents the synergistic reinforcement of PP by GF and HGB, resulting in a decreased compression modulus. However,

the compression strength increases as GF agglomerates, although this increase is gradual because GF does not bond well with the matrix. The increase in compression modulus and strength can be attributed to the addition of high-strength GF, which compensates for the reduction in mechanical performance caused by the gas within HGB. Furthermore, the inclusion of GF creates a pinning effect under external forces, which alter the direction of fracture propagation in PP matrix or even prevent cracks from turning into defects, thus enhancing the mechanical properties [24].





**Figure 7:** Relationship between GF content and compression performance: (a) compression modulus and (b) compression strength.

Excessive GF content, however, increases friction between the fibers and the polymer matrix, leading to higher shear and mixing losses in the extruder and an increase in the viscosity of the mixed system. The inhomogeneous distribution of GF in PP leads to agglomeration, which decreases the compression modulus and gradually increases the compression strength. At GF contents of 5% and 10%, the compression modulus of the composite exceeds 370MPa, meeting the criteria for insulation materials used for

deep-sea pipelines. The thermal conductivity of the HGB/GF/PP composite material is shown in Table 5, with the direct addition of GF. The thermal conductivity of the GF composite material was measured for GF contents ranging from 5% to 20%. In contrast, the mean thermal conductivity of S2 was 0.14W/m·K. These results indicate that high GF content negatively impacts both the mechanical properties and thermal insulation performance of the composite material.

**Table 5:** Thermal conductivity of group S3.

GF Percentage	Temperature (K)	Thermal Conductivity (W/m·K)	Specific Heat (kJ/kg·K)	Coefficient of Diffusion (m²/s)
0%	298.17	0.14	6.1	2.26×10 <sup>-8</sup>
5%	298.20	0.21	12.9	2.80×10 <sup>-8</sup>
10%	298.17	0.25	12.8	2.26×10 <sup>-8</sup>
15%	298.35	0.24	13.0	2.82×10 <sup>-8</sup>
20%	298.41	0.20	12.6	2.75×10 <sup>-8</sup>

Figure 8 shows the TGA curves of the composites with various GF contents of Group S3. The TGA curves indicate that the thermal decomposition temperatures of all four kinds of samples are approximately  $477~^{\circ}$ C. Given the considerable range of ambient temperatures to which deep-sea oil pipelines are subjected, selecting materials with good insulation and heat resistance is vital. Previous studies have observed that PU and polyvinyl chloride

foams exhibit thermal stability temperatures of 220 °C and 160 °C, respectively. In contrast, the thermal stability temperature of the HGB/GF/PP composite investigated herein was higher at 477 °C, suggesting its excellent thermal stability. These findings indicate that such composites can serve as effective thermal insulation and heat resistance materials in challenging environments, such as those encountered in deep-sea oil pipelines.

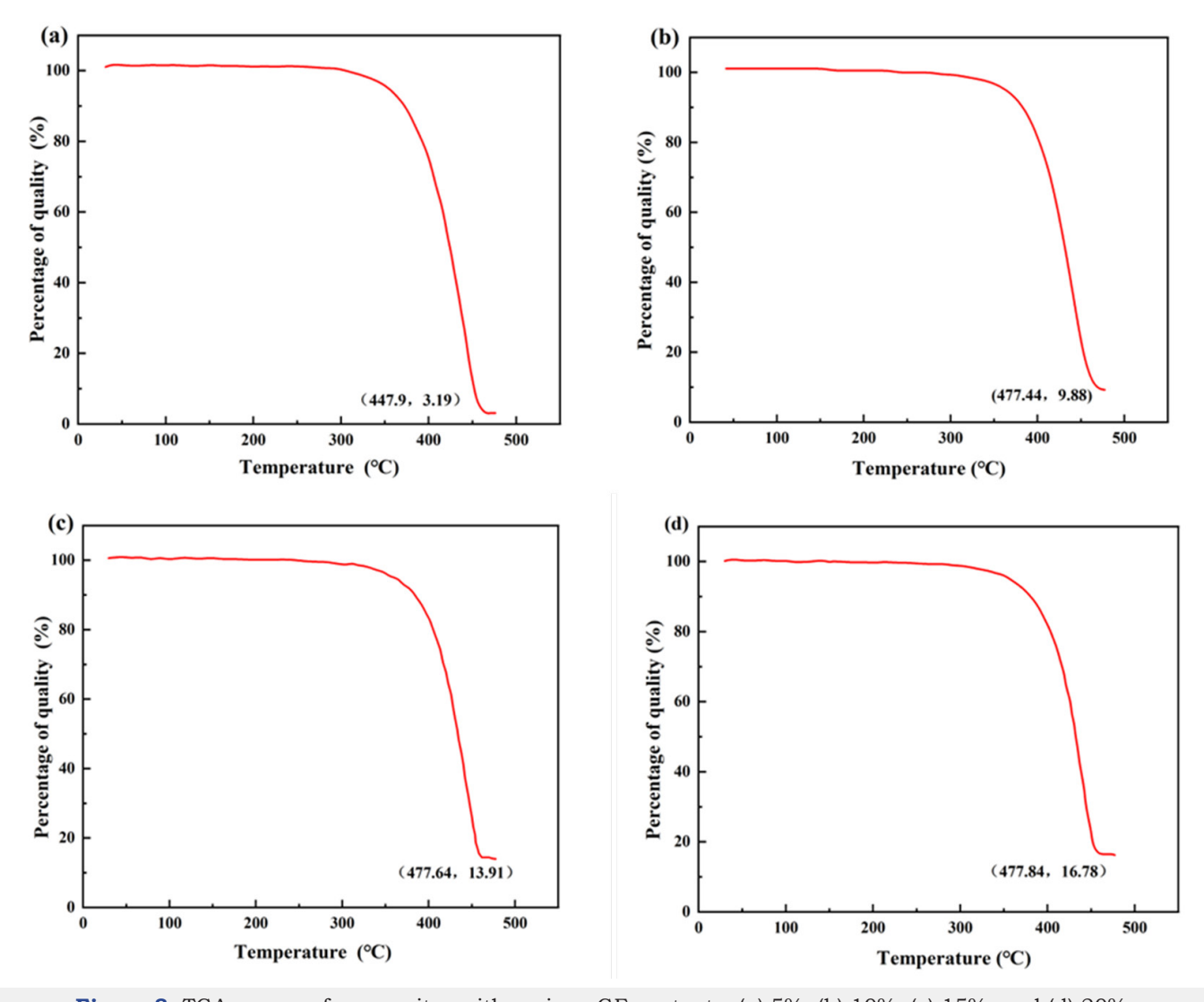


Figure 8: TGA curves of composites with various GF contents: (a) 5%, (b) 10%, (c) 15%, and (d) 20%.

## Microscopic properties and performance of group S4

The SEM images of Group S4 with various CGF contents in Figure 9 reveal that the optimized manufacturing conditions preserve the integrity and enhance the interfacial compatibility of HGB. The incorporation of a minimal amount of CGF considerably enhances interfacial compatibility, as evidenced by fibers being pulled out without breaking under external stress. At a CGF content of 3%, the bubble pore density was  $2.76 \times 108$  pores/cm³, and the

porosity decreased to 7.61% (shown in Table 6), implying that the optimal CGF content for enhancing the insulation of submarine oil pipelines belt was between 1% and 3%, potentially leading to remarkable cost savings. In addition, comparative analysis between Figure 9a & Figure 9c, at a constant CGF content, reveals that the composite containing PP-coated GF exhibited a homogeneous distribution, with no fiber pull out or aggregation throughout the manufacturing process. This uniform distribution confirms that the use of PP-coated GF effectively prevents the agglomeration.

**Table 6:** Thermal conductivity of group S4.

CGF Percentage	Temperature (K)	Thermal Conductivity (W/m·K)	Specific Heat (kJ/kg·K)	Coefficient of Diffusion (m <sup>2</sup> /s)
1%	298.2	0.15	12.9	2.80×10 <sup>-8</sup>
3%	298.17	0.12	12.8	2.26×10 <sup>-8</sup>
5%	298.35	0.09	13.0	2.82×10 <sup>-8</sup>
7%	298.41	0.17	12.6	2.75×10 <sup>-8</sup>
9%	298.17	0.04	12.8	2.80×10 <sup>-8</sup>

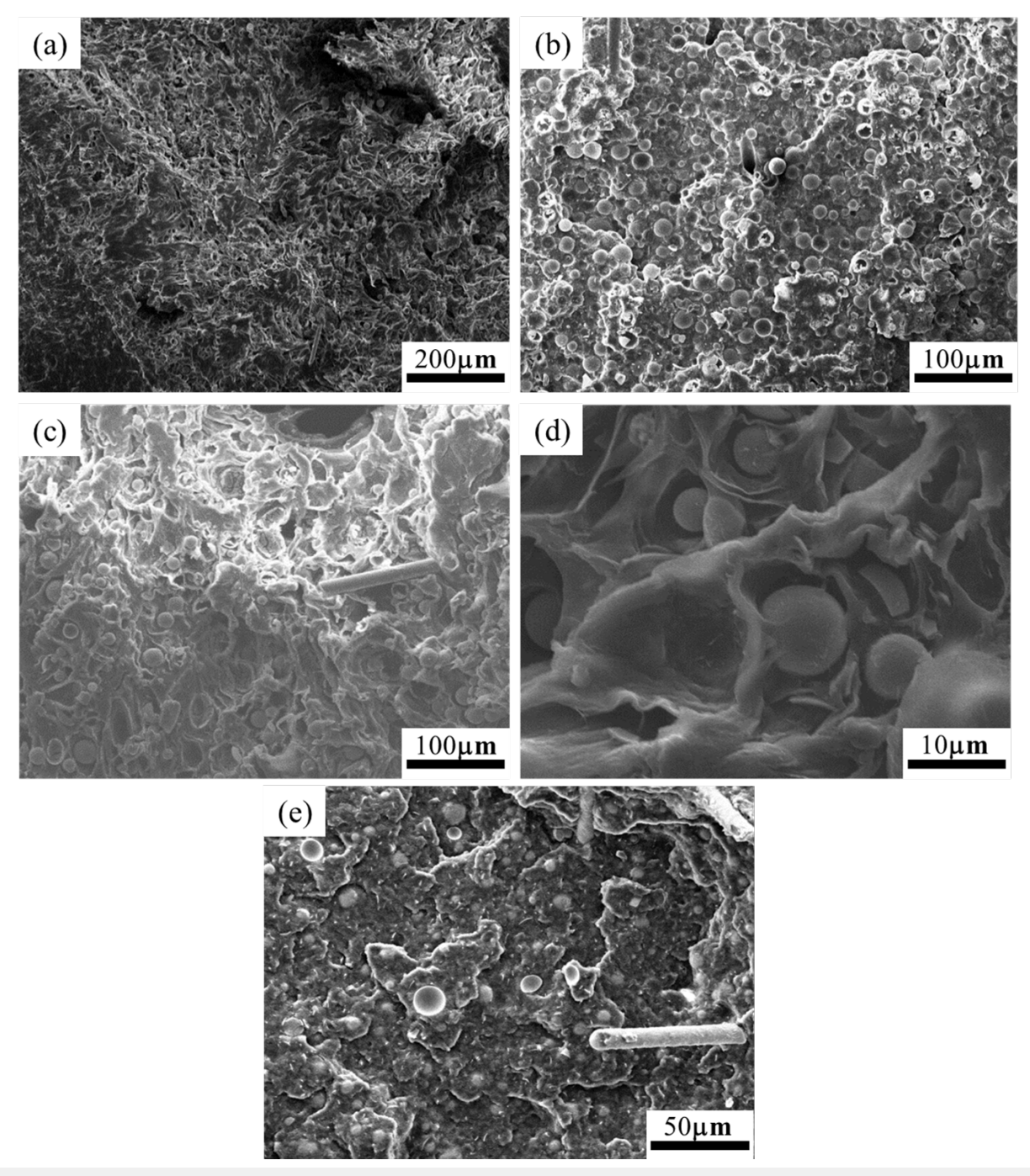
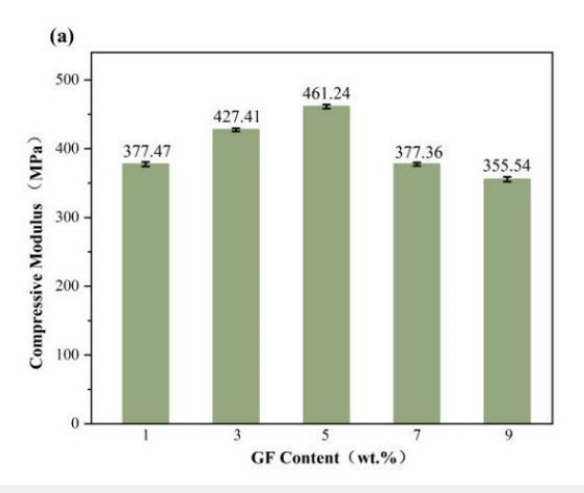


Figure 9: SEM images of composites with PP-coated GF contents: (a) 1%, (b) 3%, (c) 5%, (d) 7%, and (e) 9%.

As shown in Figure 10, both the compressive strength and modulus varied with the CGF content. The compressive strength reached its peak at 1% CGF and then decreased, while the modulus exhibited a similar trend, peaking at 3% CGF. The composite achieved its maximum compressive strength (81.14MPa) with 1% CGF and its maximum compressive modulus (461.24MPa) with 3% CGF, demonstrating a significant improvement in compression performance. This enhancement is attributed to the improved bonding between the PP-coated GF and PP matrix, which effectively addresses the issues of GF agglomeration and insufficient encapsulation. At CGF contents below 3%, the fibers are entirely

encapsulated in PP, which considerably enhances the compression performance. However, when the CGF content exceeded 3%, the compatibility with PP was reduced, hindering complete encapsulation. Consequently, under external force, the poorly bonded fibers could be pulled out or deboned from the matrix, reducing the effective load-bearing area and the compression modulus. Furthermore, the uniform dispersion of HGB within PP matrix, achieved during melt blending, allows the CGF to effectively act as a load-bearing component under external forces, thereby enhancing the mechanical properties.



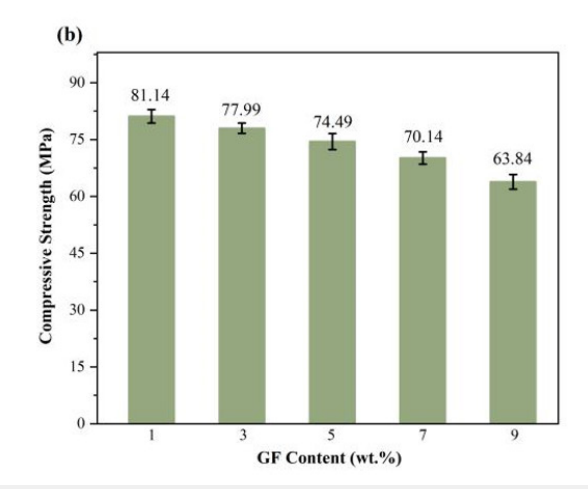


Figure 10: Effects of CGF addition method on (a) compression modulus and (b) compression strength.

## Microscopic characteristics and properties of S5

As shown in the SEM images (Figure 11a-Figure c)), the HGB and GF are poorly distinguishable, the bubble hole distribution is irregular, and apparent fractures and flaws are present in the matrix. Consequently, this disordered microstructure complicates the quantification of bubble hole parameters using ImageJ. In contrast, the industrially produced material in Figure 11d shows a notably more uniform microstructure. The composite exhibits excellent compatibility and a homogeneous dispersion of HGB. The bubble pore density increased to  $1.61 \times 10^9$  pores/cm³, and the porosity reached 17.20%, demonstrating that the HGB remained intact and well-dispersed without rupture. Moreover,

the absence of prominent fibre debonding or pull-out indicates markedly improved integration between the GF and the PP matrix. These enhanced dispersion and interfacial integration are directly responsible for the superior mechanical and insulation properties of the composite. Figure 12 shows microscopic images of the prepared material collected under natural light and sunshine at 200× magnification, revealing a uniform texture without visible impurities, voids, or defects, indicating that the material meets the quality standards required for mass production. The surface exhibits excellent hydrophobic properties and strong resistance to seawater corrosion, making the PP composite suitable for large-scale applications.

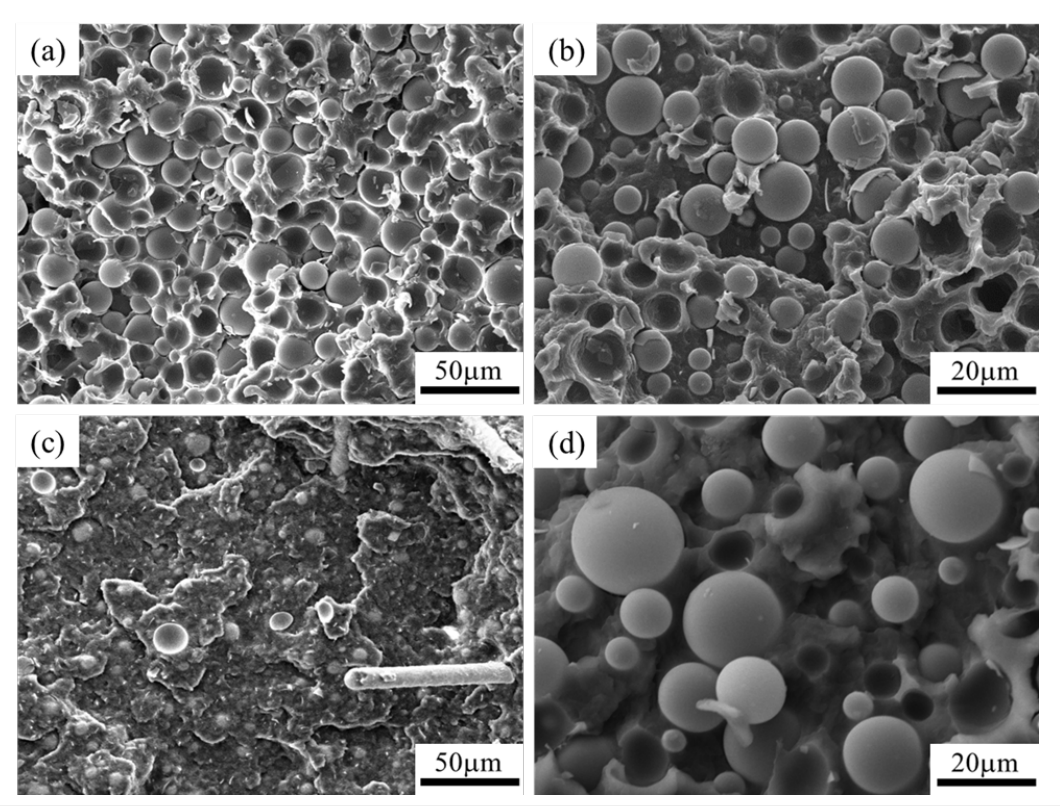
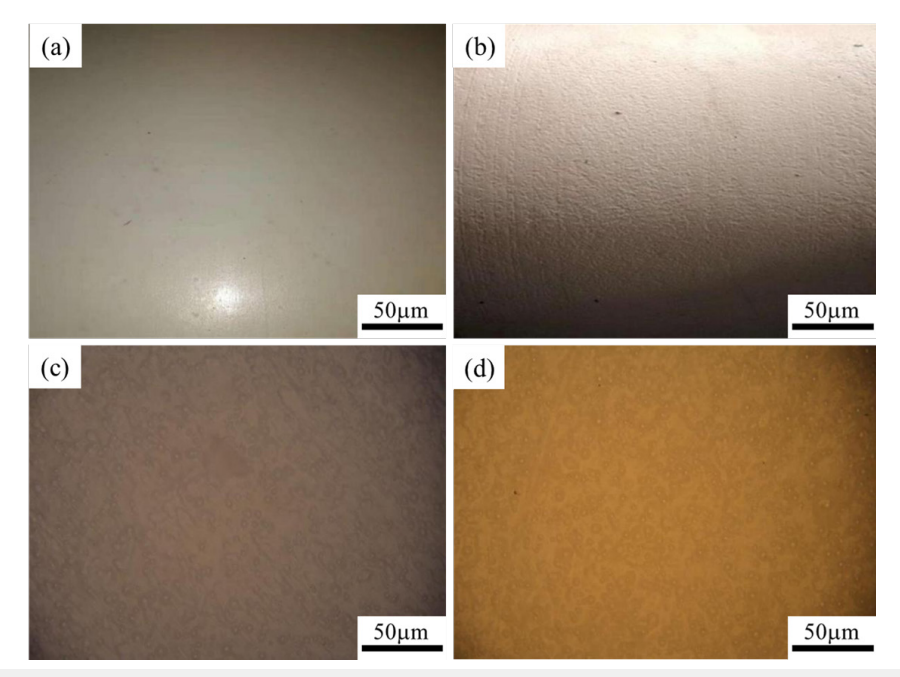


Figure 11: SEM images of industrially produced HGB/GF/PP composite: (a) overall, (b) uniformly dispersed HGB, (c) GF without debonding, and (d) local.

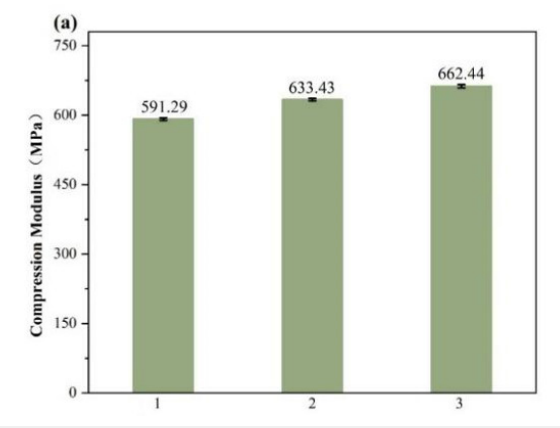


**Figure 12:** Microscope photographs of HGB/GF/PP composite: (a) and (b) top surface of composite; (c) under natural light; (d) under sunlight.

The mechanical behaviour of the composite is governed by the interaction among PP, CGF and HGB. At low HGB content, the limited number of microspheres cannot effectively buffer the applied stress, leading to their fracture and subsequent debonding of the adjacent CGF. When the HGB content is sufficiently high, they form a network that synergistically interacts with the GF/PP interfaces, enabling more effective stress transfer and allowing the CGF to bear a greater load. Thus, maintaining an adequate HGB content is crucial in this ternary system to ensure effective stress distribution and prevent premature failure [25].

Additionally, the GF acts as a nucleating agent, increasing the crystallinity of the PP matrix, which contributes to the improved mechanical stiffness. The incorporation of small-sized HGB increases the resin-filler interfacial area, which can facilitate microcrack formation and absorb a substantial amount of energy under impact, thereby enhancing toughness [26] as well. Taken random samples from different parts of the industrial products of belt for testing,

the HGB/GF/PP material comprising a mass fraction of 20% HGB and 1% CGF exhibits remarkable compression properties. Figure 13 illustrates that the mean compressive strength and compression modulus of the HGB/GF/PP material comprising 20% HGB and 1% CGF are 91.24, 629.05MPa, respectively. The tensile strength is good as well, attributed to the reinforced interface between the modified HGB and PP. The concurrent deformation of HGB and matrix under an external force increases the effective bearing area, which is beneficial for the overall composite performance. The two-step method improves the degree of uniform dispersion of HGB and GF, thereby effectively enhancing mechanical performance. Effective load transfer from the matrix to the GF through a well-bonded interface contributed to the enhanced compression properties. The essential mechanical properties of the HGB/GF/PP meet the requirements of CNOOC (China National Offshore Oil Corporation). When the aspect ratio of HGB is maintained at a constant value, the unconnected small holes (HGB) ensure a low thermal conductivity and high mechanical properties.



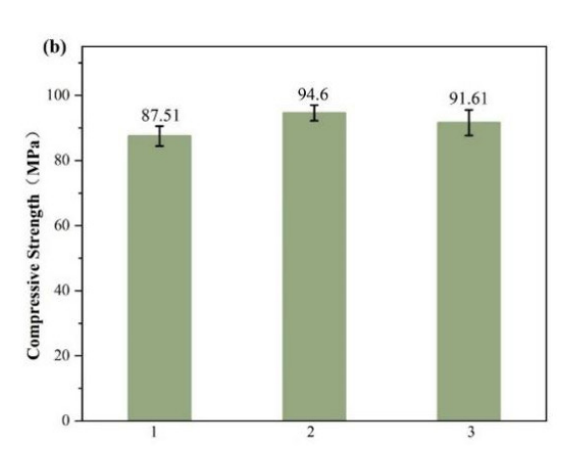


Figure 13: Compression performance of industrial products: (a) compression modulus and (b) compression strength.

As illustrated in Figure 14, the thermal conductivity tests implemented on samples from various stages of production such as initial, intermediate, and final, etc, yield a consistent value of 0.1 W/m·K. This performance considerably exceeds the thermal insulation requirements for deep-sea oil pipeline heat insulating materials (0.17 W/m·K). As illustrated in Figure 15, the successfully fabricated HGB/GF/PP composite demonstrates a remarkable synergy by simultaneously achieving high compression performance

and low thermal conductivity. This unique combination effectively bridges the performance gap between materials that are either highly insulating but mechanically weak, or mechanically strong but high thermally conductive. Consequently, this material presents significant potential for structurally integrated applications in demanding environments such as deep-sea pipeline insulation, where both load-bearing capacity and thermal insulation are critical.

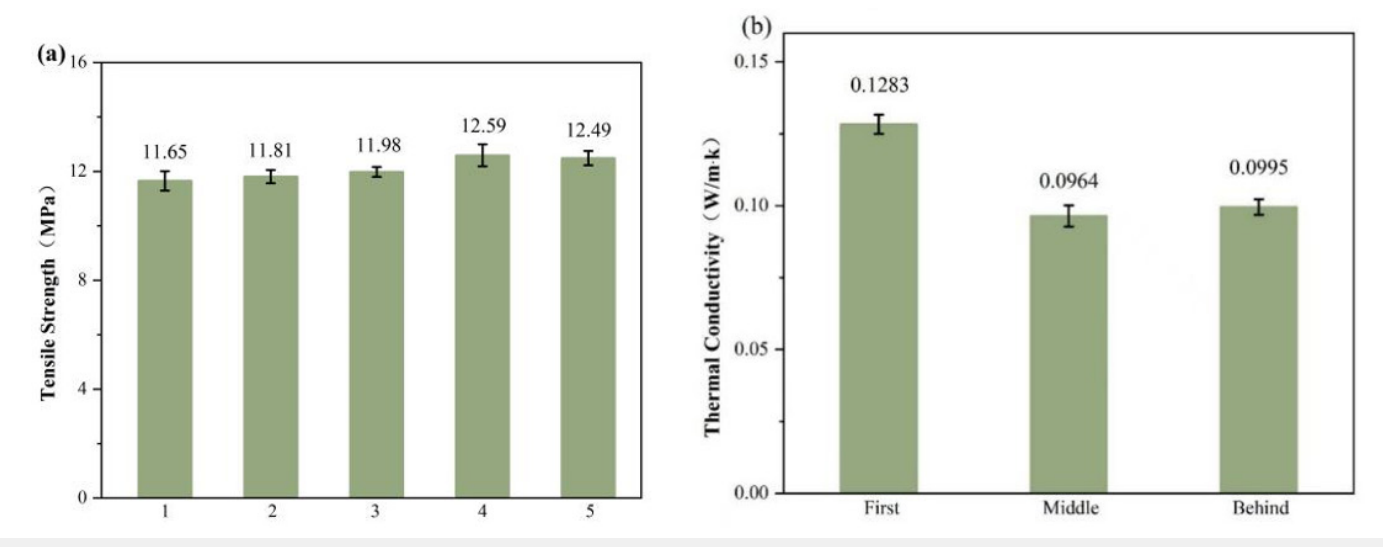
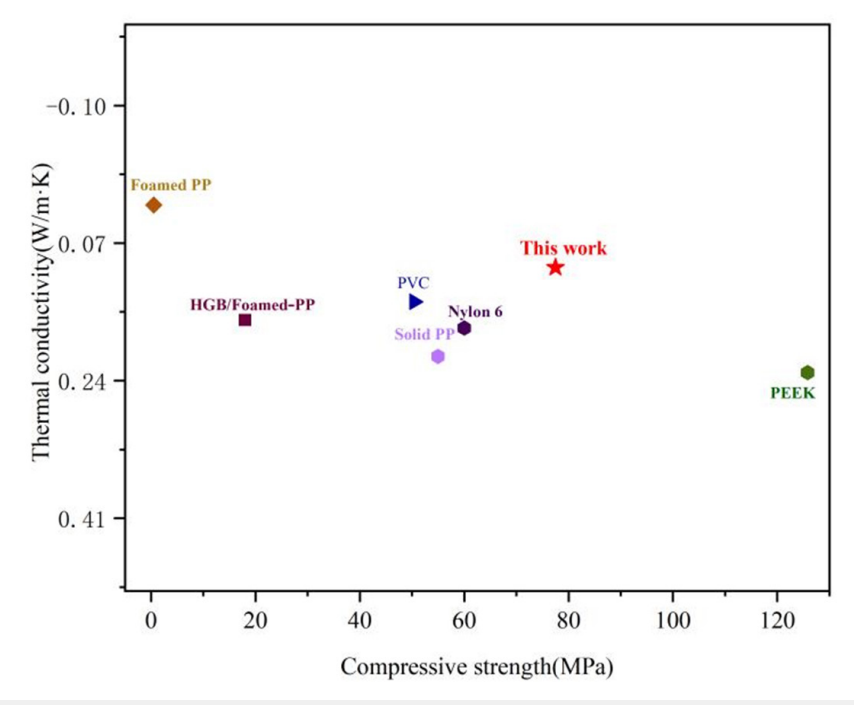


Figure 14: (a) Tensile properties and (b) thermal conductivity of industrial product belt.



**Figure 15:** The relationship between compression strength and thermal conductivity of HGB/GF/PP and other materials.

# Conclusion

HGB/PP/GF composite materials with excellent mechanical and thermal insulation properties were fabricated. After surface

modification by KH-550, the interfacial bonding between HGB and PP notably increased, and a synergistic effect occurred with GF, which considerably improved the thermal insulation and

mechanical properties of the composite material. In addition, by optimizing the processing parameters and composite components, the "two-step method" used in the factory production yielded belts with smooth and uniform surfaces and remarkably enhanced properties. With 20% HGB and 1% GF, the composite exhibited excellent mechanical properties, achieving an average compressive modulus of 629.05MPa and a compressive strength of 91.24MPa, alongside a low thermal conductivity of 0.10W/m·K. This combination of properties demonstrates the composite's strong potential for application as a thermal insulation material for deep-sea oil pipelines.

## **Author Contributions**

X.H.: Supervision, Project administration, Funding acquisition; L.W.: Writing– review & editing, Writing– original draft, C.Z.: Validation, Methodology, Investigation, Data curation, Conceptualization; D. C.: Funding acquisition; Y.Z.: Funding acquisition. M.S: Investigation, Data curation; J.M.: Writing– original draft, Data curation; J.L.: Investigation; Y.Z.: Data curation, Formal analysis.

## **Data Availability Statement**

The original contributions presented in the study are included in the article, further inquiries can be directed to the corresponding author.

### References

- Wang XH, Xie XY, Song CY, Yuan X (2021) Application and performance analysis of carbon fibber composites in deep sea oil and gas development. IOP Conference Series: Earth and Environmental Science 632(2): 022081.
- 2. Rong X, Zhu HW (2021) Thermal insulation design of subsea vertical x-mas tree. Petroleum Science 18(4): 1182-1194.
- 3. Tsapko Y, Kasianchuk I, Likhnyovskyi R, Tsapko A, Kovalenko V, et al. (2023) Determining thermal and physical characteristics of wood polymer material for pipeline thermal insulation. Eastern-European Journal of Enterprise Technologies 5(10): 63-72.
- Alnaimat F, Ziauddin M (2020) Wax deposition and prediction in petroleum pipelines. Journal of Petroleum Science and Engineering 184: 106385.
- Yao ZM, Zhang YY, Zheng YZ, Xing CH, Hu Y (2022) Enhance flows of waxy crude oil in offshore petroleum pipeline: A review. Journal of Petroleum Science and Engineering 208(PC): 109530.
- Praveenkumara J, Madhu P, Yashas Gowda TG, Sanjay MR, Siengchin S (2022) A comprehensive review on the effect of synthetic filler materials on fiber-reinforced hybrid polymer composites. The Journal of The Textile Institute 113(7): 1231-1239.
- Yang J, Lourenço MI, Estefen SF (2018) Thermal insulation of subsea pipelines for different materials. International Journal of Pressure Vessels and Piping 168: 100-109.
- 8. Li XR, Zheng T, Wang XD, Zhang XH, Qiao YJ (2024) Research progress of epoxy resin composites toughened using thermoplastic resin. Journal of Harbin Engineering University 45(4): 808-818.
- Lu JJ, Guan JP, Wang HQ, Dang RQ, Fan MX, et al. (2022) Investigation on compressive and impact performance of GO-modified hollow glass beads/epoxy resin composites in simulated deep-sea environment. Composites Science and Technology 227: 109608.

- Antunes M, Mudarra M, Velasco JI (2011) Broad-band electrical conductivity of carbon nanofibre-reinforced polypropylene foams. Carbon 49(2): 708-717.
- Grealish F, Roddy I (2002) State-of-the-art on deep water thermal insulation systems. International Conference on Offshore Mechanics and Arctic Engineering 36134: 339-347.
- 12. Wang X, Shi H, Li YP, Chen SY, Li YF, et al. (2024) Preparation and interfacial properties of multifunctional polypropylene/hollow glass bead composites. Surfaces and Interfaces 46: 103921.
- 13. Sekhar CM, Reddy PB, Kuchi C, Basha CK, Al-Zahrani FAM, et al. (2024) Enhanced solar-driven photocatalytic hydrogen production, dye degradation, and supercapacitor functionality using MoS<sub>2</sub>-TiO<sub>2</sub> nanocomposite. Ceramics International 50(20): 38679-38687.
- 14. Mangiri R, Ramachandran T, Anil Kumar Y, Ghosh A, Al-Sehemi AG, et al. (2025) Surface engineering of  $\rm M_5X_4$  MXenes for next-gen energy solutions. Materials Today Chemistry 48: 102864.
- 15. Ai W, Liu S, Zhang J, Miao S, Wei C (2019) Mechanical and nonisothermal crystallization properties of coal gasification fine slag glass bead-filled polypropylene composites. Journal of Applied Polymer Science 136(30): 47803.
- 16. Carvalho GB, Canevarolo SV, Sousa JA (2020) Influence of interfacial interactions on the mechanical behavior of hybrid composites of polypropylene/short glass fibers/hollow glass beads. Polymer Testing 85: 106418.
- 17. Guo YB, Zhang Z, Cao ZQ, Wang DG (2019) Wear behavior of hollow glass beads (HGB) reinforced nitrile butadiene rubber: Effects of silane coupling agent and filler content. Materials Today Communications 19: 366-373.
- Zhai GJ, Ding Y, Ma Z, Wei ZH, Li X, et al. (2022) Novel triaxial experimental investigation on compressive behavior of hollow glass microspheres composites under varied temperature environments. Polymer Testing 115: 107745.
- 19. Li TQ, Qu MJ, Zheng LJ, Zhu SY, He LL (2014) Influence of technological conditions on cell structure of supercritical carbon dioxide foaming material. China Synthetic Resin & Plastics 31(1): 71-75.
- Khoshkava V, Kamal MR (2014) Effect of drying conditions on cellulose nanocrystal (CNC) agglomerate porosity and dispersibility in polymer nanocomposites. Powder Technology 261: 288-298.
- 21. Xiao CG, Li DX, Zeng D, Lang F, Xiang Y, et al. (2021) A comparative investigation on different silane coupling agents modified sericite mica/polyimide composites prepared by in situ polymerization. Polymer Bulletin 78: 863-883.
- 22. Gil BM, Song SW, Lee JH, Jeon J, Lee KH, et al. (2019) Introduction of primary chemical bonding in lignin-based PP composites for mechanical reinforcement via reactive extrusion. Composites Part B: Engineering 165: 510-515.
- 23. Chen MJ, Zhang Y, Zhang X (2004) Recent research progress of short glass fiber reinforced polypropylene. China Plastics 18 (8): 3-8.
- 24. Lu JJ, Dang RQ, Zhang W, Chernysh Y, Wang HQ, et al. (2023) Investigation on preparation and mechanical properties of carbon fiber fabric/ hollow glass microspheres/epoxy resin sandwich composite laminates. Polymer Composites 44(1): 356-364.
- 25. Duan HD, Wang CY, Wang LJ, Jiang TH, He L, et al. (2016) Mechanical properties of polypropylene/fiber composite foaming materials under the condition of three-phase existing. Polymer Materials Science and Engineering 32(2): 71-77.
- 26. Li JW, Song L, Han L, Zhang BH, Feng YK (2016) Influence of hollow glass microspheres modified by a rare-earth/titanium coupling agent on the nonisothermal crystallization of polypropylene. Journal of Macromolecular Science, Part B 55(4): 372-381.